Journal of Power Sources 196 (2011) 6644–6650

Contents lists available at ScienceDirect

Journal of Power Sources

journal homepage: www.elsevier.com/locate/jpowsour

Electrochemical mechanisms in tin-containing composite materials for negative electrodes in Li-ion batteries: Transformation of the interfacial tin species during the first galvanostatic discharge of $Sn[BPO_4]_{0.4}$

Donato E. Conte [a,*], Lorenzo Stievano [a,**], Josette Olivier-Fourcade [a], Jean-Claude Jumas [a], Patrick Willmann [b]

[a] Institut Charles Gerhardt - AIME, Université Montpellier 2, 34095 Montpellier, France
[b] CNES, Centre Spatial de Toulouse, 31401 Toulouse, France

ARTICLE INFO

Article history:
Received 25 November 2010
Received in revised form
23 December 2010
Accepted 24 January 2011
Available online 2 February 2011

Keywords:
Li-ion batteries
Anode materials
Tin-based composites
Mössbauer spectroscopy

ABSTRACT

The $Sn[BPO_4]_{0.4}$ composite material is composed of three main constituents: the electrochemically active Sn^0 species, the BPO_4 buffer matrix, and an interfacial amorphous Sn^{II} borophosphate phase which acts as a link between the other two, improving the cohesion of the whole composite. In this paper, we report an investigation of the effect of the reaction time on structure and size of this interfacial layer formed between the Sn^0 and the BPO_4 particles. ^{119}Sn Mössbauer spectroscopy shows an increase in the amount of the oxidized Sn^{II} species with the increase of the reaction time following a quasi-kinetic profile. *Operando* Mössbauer spectroscopy allowed the study of the transformation of the interface at the beginning of the first electrochemical cycle, indicating that the big irreversible loss during the first discharge is closely related to the increase of the amount of Sn^{II} in the amorphous interface.

1. Introduction

The interest in substituting graphite as the anodic material in Lithium-ion batteries has risen since the announcement of the Fujifilm amorphous tin-based composite oxide (ATCO) made in 1997 [1]. These composites showed an acceptable cyclability but a very fast capacity fading down to values equal to 1/3 of that of graphite (372 mAh g^{-1}) [2].

More recently, new composites based on tin were proposed, in which the metal has been nanostructured, carbon coated, carbon enrobed, nanotube encapsulated or used to produce Sn–M binary alloys (where M can be Sb, Co, Fe, etc.) with excellent electrochemical performances [3]. Among these new materials, our group has proposed a tin metal composite where tin is dispersed into a buffer matrix. In these materials, the key factors for the matrix to be effective are: (i) possibility to chemically react with Sn in order to establish a conductive interface assuring the material cohesion, (ii) capacity to accommodate the additional volume produced by the typical volume expansion of tin during the Li–Sn alloying process and (iii) lightness relative to the metal not to affect the theoretical and effective capacity of the final composite material. Among other possible candidates, BPO_4 [4–7] Na–B–PO_x glass [6] and $CaSiO_3$ [4,8] have proven to be interesting matrixes for tin based composites.

For these materials, the thorough physico-chemical description of the synthesis process, involving the formation of a tin–matrix interface containing characteristic divalent tin species, is essential for the production of better and more optimized anodic materials. In this paper, an improved model of the tin–matrix interface in Sn–BPO_4 is proposed compared to the one previously proposed by Aboulaich et al. [5] on the basis of new information gathered mainly by Mössbauer spectroscopy (*in situ* and *operando*) on novel materials prepared using different reaction times.

2. Experimental

2.1. Materials

The $Sn[BPO_4]_{0.4}$ composite was prepared by a two-steps solid state reaction method. In a first step, BPO_4 was synthesized from equimolar amounts of $NH_4H_2PO_4$ and H_3BO_3 (both from Acros Organics). The starting materials were ground in an agate mortar and placed in an alumina crucible. De-ionized water was added in

* Corresponding author.
** Corresponding author. Tel.: +33 467143346; fax: +33 467143304.
E-mail addresses: iguanasornione@libero.it (D.E. Conte), lorenzo.stievano@univ-montp2.fr (L. Stievano).

0378-7753/$ – see front matter © 2011 Elsevier B.V. All rights reserved.
doi:10.1016/j.jpowsour.2011.01.091

order to form a homogeneous white paste which was heated in a furnace to 380 °C for about 13 h.

In the second step, BPO_4 was mixed with Sn powder (Aldrich) in the desired molar ratio. This mixture was heated in a vitreous carbon vessel inside a horizontal tube furnace to 500 °C in a constant flow of high purity nitrogen gas and was then rapidly quenched to room temperature by removing the vessel from the furnace. It must be noted that similar syntheses performed in a flow of high purity Ar, 5% H_2/Ar or 5% H_2/N_2 lead to virtually identical materials (data not shown). Final grinding at room temperature gives the final grey composite powder.

Several samples were synthesized using the same batch of BPO_4 as the starting material but varying the reaction time between 1 and 28 h (cf. Fig. 2).

2.2. Methods

The samples were characterized by X-ray powder diffraction (XRD) using a PHILIPS Gonio diffractometer. The pattern was recorded in the Bragg–Brentano θ–2θ continuous mode using CuK_α radiation (λ = 1.5418 Å).

^{119}Sn transmission Mössbauer spectra (TMS) were recorded with both source and absorber at room temperature in the constant acceleration mode using components manufactured by ORTEC and WISSEL and a source of $Ca^{119m}SnO_3$ with a nominal activity of 370 MBq. The velocity scale was calibrated with the magnetically split sextet spectrum of a high-purity α-Fe foil as the reference absorber, using a ^{57}Co(Rh) source. The spectra were fitted with appropriate combinations of Lorentzian profiles by the least-squares method using the ISOfit program [9], and the goodness of fits was controlled by a classical χ^2-test. Hyperfine parameters such as isomer shift (δ), quadrupole splitting (Δ), relative resonance area of the sub-spectra (*S.F.*) and effective molar fractions (*E.F.*) calculated taking into account the Lamb–Mössbauer factors of the observed tin species are reported in Table 1 All isomer shifts are given with respect to the room temperature spectrum of $BaSnO_3$.

Electrochemical tests were carried out on standard Swagelok™ cells built with a cathode containing 90 wt% Sn–BPO_4 composite sample and 10 wt% carbon black electronic conductor, pure lithium metal as the anode, and 1 M $LiPF_6$ in a mixture of propylene carbonate (PC), ethylene carbonate (EC) and dimethyl carbonate (DMC) with a molar ratio of 1:1:3 as the electrolyte. The complete cells, schematized as follows

$$\mathrm{Li}\,\big|\,1\ \mathrm{M\ LiPF_6\ in\ PC:EC:DMC(1:1:3)}\,\big|\,\mathrm{Sn[BPO_4]_{0.4}}$$

were assembled in an argon-filled glove box. The cells were tested using a VMP® system (Bio-Logic) in the galvanostatic mode with a 0.01–1.2 V vs. Li^+/Li^0 potential window at C/5 rate (a C/*n* rate expresses the equivalent current density necessary for the reaction of 1 mol of Li^+ per mole of active material in *n* hours. A C/5 rate represents the current density necessary for the reaction of 1 mol of Li^+ per mole of active material in 5 h).

The detailed investigation of the composite material during cycling by *operando* ^{119}Sn Mössbauer spectroscopy was made possible by the development of a specific electrochemical cell allowing the measurement of the Mössbauer spectra during the reaction vs. Li metal. This cell is the adaptation of an electrochemical cell formerly developed for *operando* X-ray diffraction and X-ray absorption spectroscopy [10] studies. In order to allow the registration of a sufficient number of spectra with an acceptable signal-to-noise ratio, the *operando* electrochemical cell was employed using the same VMP® system under the same experimental conditions employed for normal Swagelok cells, but using instead a C/30 rate (1 mol of Li reacted in 30 h). In this way, a spectrum could be registered in a 3 h period

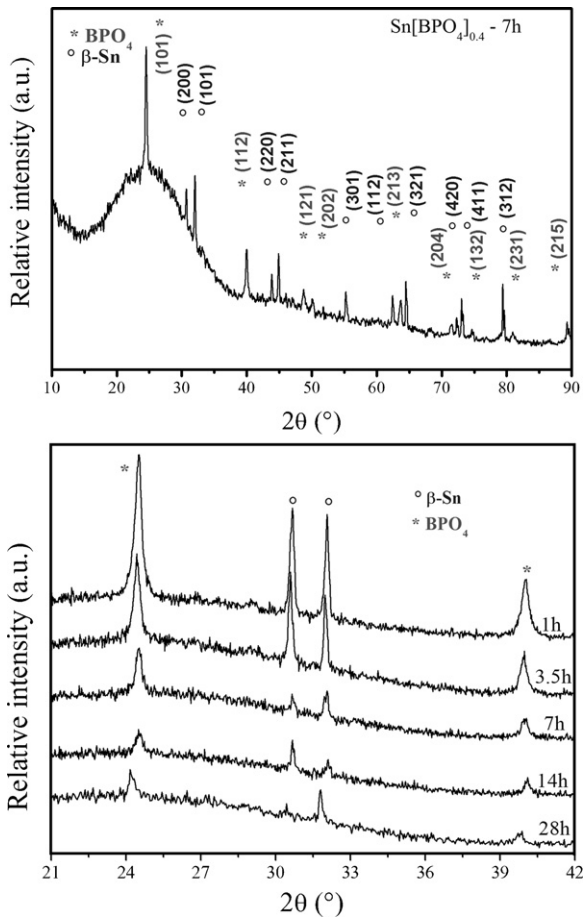

Fig. 1. X-ray diffraction patterns of the reference $Sn[BPO_4]_{0.4}$ composite material obtained with a reaction time of 7 h (up) and detail of the XRD patterns of the composites obtained at different reaction times (down).

thus corresponding to the reaction of 0.1 mol of Li per mole of tin.

3. Results and discussion

3.1. $Sn[BPO_4]_{0.4}$ composites: effect of the reaction time on the composition

The XRD patterns of the reference composite material obtained with a reaction time of 7 h and of the other composites with the same composition but prepared at different reaction times are shown in Fig. 1 (up and down, respectively).

The diffraction patterns observed for all the composites are those of pure β-Sn and BPO_4. Indexation and cell parameters determination were performed elsewhere [7]. In the enlargements reported in Fig. 1, it is possible to discern the influence of the reaction time on the resulting composite obtained with a reaction time of 7 h. When the reaction time does not exceed 3.5 h, BPO_4 and β-Sn reflections vary only slightly in intensity and are always at the same positions, indicating a very partial chemical reaction between the two components. At increasing reaction times, both sets of reflections decrease progressively in intensity even if positions remain virtually unchanged. After 28 h, the diffraction lines of both components are very difficult to identify and the tin (2 0 0) reflection is totally lost. Note that patterns in Fig. 1 (down) are plotted using the same intensity scale.

The ^{119}Sn Mössbauer spectra of the samples obtained after different reaction times are shown in Fig. 2, while the corresponding

Table 1
^{119}Sn Mössbauer parameters at room temperature for the $Sn[BPO_4]_{0.4}$ prepared with different reaction times.

Sample	Tin species	δ [mm s^{-1}]	Δ [mm s^{-1}]	*S.F.* [%]	*E.F.* [%]
β-Sn (Aldrich)	Sn^0	2.54(2)	0.24(4)	100	100
1 h	Sn^0	2.55(2)	0.36(2)	61(2)	73
	Sn^{II}	3.29(3)	1.66(5)	39(2)	**27**
3.5 h	Sn^0	2.55(2)	0.36(2)	48(2)	61
	Sn^{II}	3.28(2)	1.71(3)	52(2)	**39**
7 h	Sn^0	2.55(2)	0.36(2)	42(1)	56
	Sn^{II}	3.22(1)	1.70(2)	58(1)	**44**
10 h	Sn^0	2.55(2)	0.36(2)	38(1)	51
	Sn^{II}	3.22(1)	1.68(2)	62(1)	**49**
14 h	Sn^0	2.55(2)	0.36(2)	32(1)	45
	Sn^{II}	3.25(1)	1.73(2)	68(1)	**55**
20 h	Sn^0	2.55(2)	0.36(2)	31(2)	44
	Sn^{II}	3.29(2)	1.71(3)	69(2)	**56**
28 h	Sn^0	2.55(2)	0.36(2)	14(1)	22
	Sn^{II}	3.32(1)	1.67(2)	86(1)	**78**

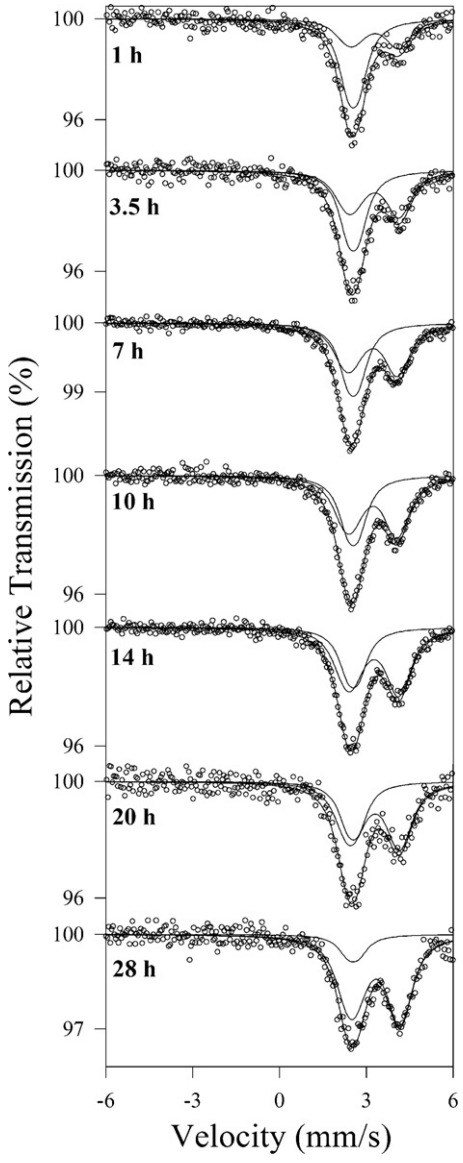

Fig. 2. Room temperature ^{119}Sn Mössbauer spectra of the $Sn[BPO_4]_{0.4}$ composites at increasing reaction times.

hyperfine parameters are listed in Table 1. In agreement with the X-ray diffraction patterns, the Mössbauer spectra of the composite materials show a net decrease in relative intensity of the spectral component representing tin metal with increasing reaction times. This decrease corresponds to the emergence of a new spectral component with hyperfine parameters typical of Sn^{II} [11–15], and previously attributed to divalent tin species formed at the interface between the tin metal particles and the BPO_4 matrix [4–8,16,17]. As already specified in the previous publications, the formation of divalent tin is rather unexpected, since this reaction occurs in flowing N_2, in the absence of oxygen. In order to better understand this result, the reaction was repeated several times in an alternative atmosphere (in flowing Ar, 5% H_2/Ar, and 5% H_2/N_2), producing practically the same result (data not shown). Even though the exact species that is reduced allowing the formation of Sn^{II} could not be identified, it can be observed that the formation of divalent tin always goes along with the amorphisation of BPO_4 during the annealing step at 500 °C, leading to the formation of a glass-like phase. This result suggests that divalent tin can only be formed by the reaction of tin metal with the borophosphate matrix.

It must be noted that the redox potentials of the different species involved in the solid state reaction at 500 °C, *i.e.*, borate, phosphate and tin, are unknown and difficult to establish [18], and thus a precise chemical reaction involving a simple phosphate and/or borate reduction cannot be written. However, it must be noticed that, on the one hand, boron can adopt both a three or four fold coordination environment in borates (boron polyoxoanions), affording greater variety in redox potential adjustment [19]. On the other hand, an increasing reducibility of borate species are known to occur at relatively high potentials in borate glass melts at high temperatures [20]. Species such as borates (but similar consideration can possibly be advanced for phosphates, which can be reduced to phosphites) might thus be responsible for the reduction of tin under our reaction conditions.

Finally, the formation of borophosphate glasses goes along with the formation of ring-like structures carrying a delocalized negative charge, including both borate and phosphate species [21,22]. It cannot be excluded that the formation of such very stable mixed species is the driving force allowing for the oxidation of tin.

Considering that the hyperfine parameters of the metallic tin component are not expected to vary sensibly with the reaction time, a specific fitting procedure of the Mössbauer spectra has been employed along this series of samples: the spectra have been fitted all at the same time, and the parameters of tin metal were allowed to vary in the same way in all the spectra while the divalent tin parameter were left free to vary independently (Table 2). This procedure allows one to better describe the tin metal component when

Table 2
Summary of the electrochemical behavior of selected $Sn[BPO_4]_{0.4}$ composites (cf. Fig. 5).

Synthesis time	1st cycle loss	1st cycle capacity ($mAh\,g^{-1}$)
1 h	1.3 Li^+ (35%)	608
7 h	1.6 Li^+ (32%)	799
14 h	1.7 Li^+ (48%)	563
28 h	2.2 Li^+ (51%)	721

it is very weak in intensity and difficult to localize with precision, and consequently to reduce the error in the determination of the hyperfine parameters of the divalent tin spectral component and of the relative resonance areas of the two species. In addition, a Gaussian distribution of isomer shifts with correlated quadrupole splittings was employed to fit the component representing divalent tin in the amorphous interface; as already observed for tin containing glasses, tin is expected to be present in a variety of coordination environments not very different among them, giving rise to a noticeable line broadening and to the appearance of a slight asymmetry of the Mössbauer doublet.

The results of this fit give Sn^{II} components with virtually the same hyperfine parameters for all spectra and increasing intensity relative to the metallic tin component, which becomes very weak in the samples obtained with long reaction times (>20 h). These hyperfine parameters are not very different from those observed for divalent tin in borophosphate glasses with average composition $(SnO)_{0.6}(B_2O_3)_{0.19}(P_2O_5)_{0.19}$ (J. Chouvin et J.-C. Jumas, unpublished data). Since both isomer shift and quadrupole splitting are rather sensitive to the divalent tin content in the glass phase, this results shows that the coordination of tin in the interface is rather homogeneous, and that the local concentration of tin in the interface does not vary significantly throughout the advancement of the reaction.

Taking into account the Lamb–Mössbauer factors at room temperature of the two tin species, previously determined in Refs. [7,23] (f = 0.07 and 0.12 for tin metal and divalent tin in the interface, respectively), one obtains directly their relative atomic abundances, which are reported in Fig. 3 against the reaction time. A progressive increase of the relative amount of the Sn^{II} species is observed, reaching 71% of the total tin content after 28 h of reaction. Considering that in this last sample the borophosphate matrix has almost completely reacted with tin, as shown by the X-ray diffraction results, and taking into account the uncertainty in the values of the Lamb–Mössbauer factors for the badly defined divalent tin species, this final composition agrees reasonably well with the observed hyperfine parameters of the divalent tin component. This last sample can thus be considered as a composite made of a small amount of tin metal and a larger fraction of purely amorphous ATCO-type compound.

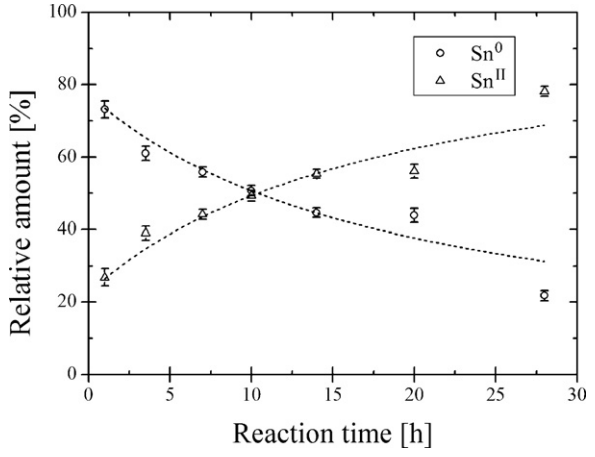

Fig. 3. Variation of the effective fraction in the Sn^0 and Sn^{II} content in $Sn[BPO_4]_{0.4}$ composites with the reaction time. The lines are meant as a guide to the eye.

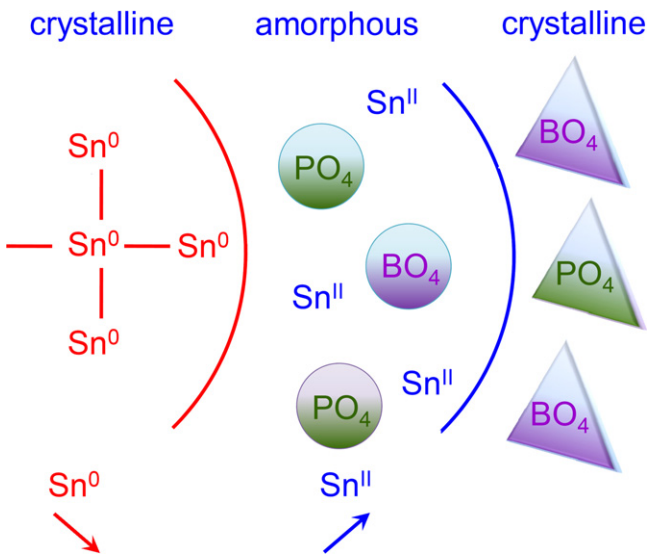

Fig. 4. Model of the $Sn[BPO_4]_{0.4}$ composite material schematizing the formation of a Sn–BPO_4 interface between the tin metal particles and the BPO_4 matrix. The increasing and decreasing arrows relative to the Sn species represent the increasing reaction time.

By combining the results of X-ray diffraction, showing a decrease of the tin metal content and of the crystalline borophosphate with reaction time, and the Mössbauer data revealing a simultaneous increase of the amount of divalent tin in the amorphous phase, a new model of the structure of the composite emphasizing the presence of an amorphous interface between the tin metal particles and the buffer matrix can be proposed (cf. Fig. 4.)

3.2. Electrochemical behavior of the $Sn[BPO_4]_{0.4}$ composites

3.2.1. General electrochemical response

The galvanostatic response against lithium metal at C/5 (one lithium inserted each 5 h) of four representative $Sn[BPO_4]_{0.4}$ composites obtained at different reaction times from 1 h to 28 h is reported in Fig. 5, whereas the electrochemical behavior after the first cycle for all the studied samples are summarized in Table 2.

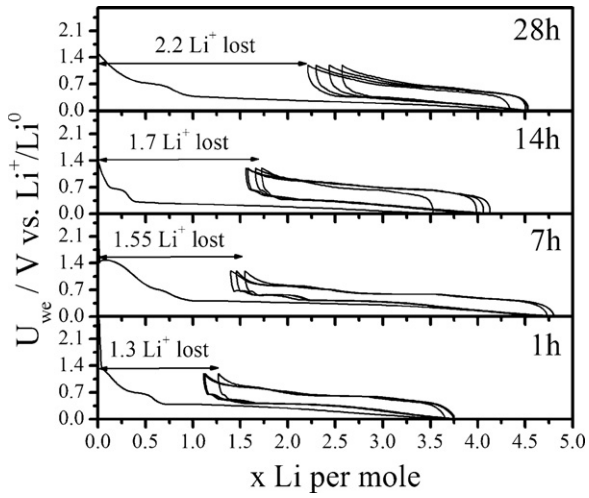

Fig. 5. Galvanostatic cycling curves at C/5 for the $Sn[BPO_4]_{0.4}$ composites obtained with reaction times of 1 h, 7 h, 14 h and 28 h in the potential window between 0.0 and 1.2 V vs. Li^+/Li^0.

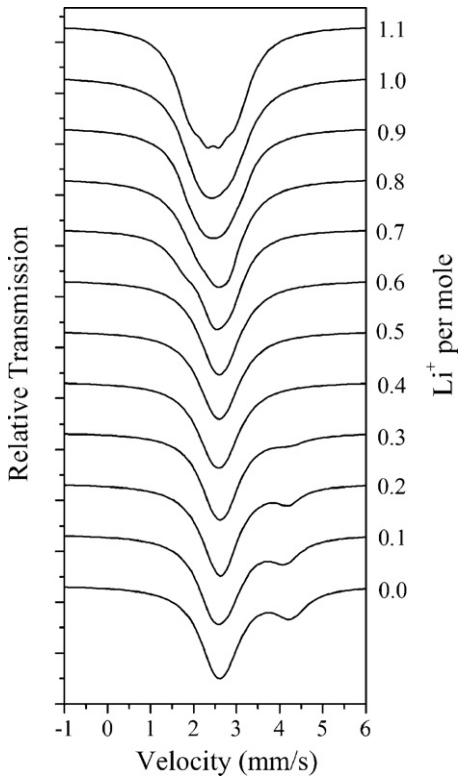

Fig. 6. Evolution of the *operando* ^{119}Sn Mössbauer spectra at room temperature with the amount of reacted Li^+.

The first discharge process against lithium metal of the different composites is rather similar, showing in the first part of the discharge (between 0 and about 1 inserted Li) a certain number of short plateaus at different potentials between 1.5 and 0.5 V against Li^+/Li^0. These signals are followed by a very long plateau which continues until the complete discharge. The length of this plateau varies sensibly with the reaction time employed for preparing the composite, and is the longest for the sample prepared at 7 h, which apparently allows the insertion of the largest amount of lithium among the prepared samples. With increasing reaction time, a progressive shortening of the typical Li–Sn reaction plateau is then observed.

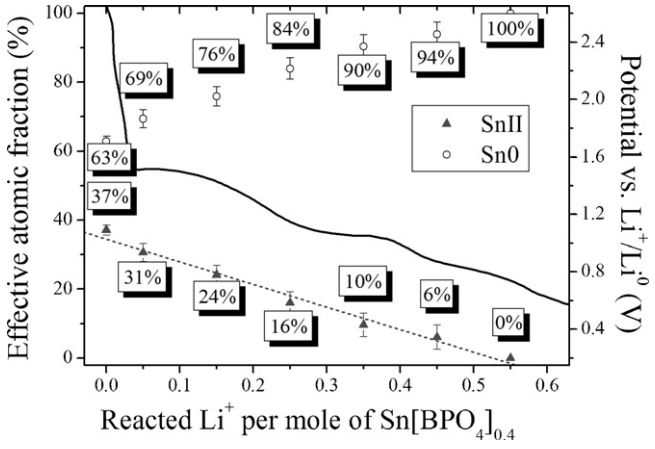

Fig. 7. Zoom of the first galvanostatic discharge curve of $Sn[BPO_4]_{0.4}$ composite at C/30 rate together with the variation of the relative amounts of the tin species. Percentages obtained from the relative areas of the Mössbauer subspectra corrected by the Lamb–Mössbauer factor according to the procedure detailed in Ref. [7].

The length of the long plateau below 0.5 V, which corresponds to the progressive formation of the Li–Sn alloys, probably depends on the accessibility of tin metal to accept the insertion of Li; in fact, Li insertion occurs only when an electrical connection between the Sn particles and the current collector exists. In this case, the transformation of part of the pristine crystalline matrix into a Sn(II)-containing amorphous interface by reaction with a small portion of tin metal seems to stabilize the tin metal particle, strongly improving the electronic conductivity between tin metal particles and the electric circuit. Too short reaction times produce samples containing not enough glassy matrix, and thus poor conductivity, leaving a significant portion of the tin metal particles electrochemically inactive. Too long reaction times, on the other hand, transform a too large portion of the tin into Sn(II), and the subsequent reduction produces large and badly connected tin metal particles.

It is worth noting that a plateau at 1.3 V, commonly assigned to the reduction of divalent tin to tin metal, is observed only in the sample heated for 7 h, and it is not observed in the samples heated for longer times and thus containing more divalent tin, as previously shown by Mössbauer spectroscopy (*vide supra*). This discrepancy can be explained by the fact that the reduction of divalent tin is not only observed on a biphasic plateau, but continues regularly down to about 0.6 V together with other reactions (namely, reaction with the electrolyte leading to the formation of the SEI layer and beginning of formation of the Li–Sn alloys), as it will be shown by the detailed *operando* study of this part of the discharge for the sample prepared with a reaction time of 7 h (vide infra, Section 3.2.2). This fact is not surprising, considering that the reduction of tin goes along with its extrusion from the amorphous matrix to form metal particles, which might induce a variable polarization of the discharge curve depending on the depth of the extrusion process. The amount of Li irreversibly lost for reducing Sn^{II} is better reflected by the irreversible capacity measured at the end of the first charge/discharge cycle. In fact, this value increases regularly with the reaction time, and correlates rather well with the increase in divalent tin content in the starting composite.

During the following electrochemical cycles, the typical well-defined potential curve with different plateaus is observed. This curve, which can be interpreted in terms of formation/reaction of a series of Li–Sn compositions by comparing the experimental data to the *ab initio* calculated potential for each system [24,25], begins to lose in definition starting from the sample obtained with a reaction time of 14 h, to become an almost smooth curve after 28 h of reaction.

In summary, the sample obtained with a reaction time of 7 h provides the best delivered capacity, *i.e.*, the best electrochemical accessibility of the tin metal. At the same time, this sample presents a still acceptable first-cycle loss, and offers thus the best compromise in terms of global electrochemical performances. In the following section, the chemical mechanisms occurring during the first part of the first discharge (from 0 to about 1.2 Li reacted per mole of Sn in the sample) of this sample are investigated in detail by *operando* Mössbauer spectroscopy, in order to understand more precisely the nature of the processes related to the first-cycle irreversible loss of this family of materials.

3.2.2. Study of the 0 → 1.2 reacted Li region by operando Mössbauer spectroscopy

In order to obtain a sufficient number of spectra to describe in detail the different parts of the discharge, the *operando* cell was discharged at C/30, *i.e.*, a speed noticeably lower than the one used for the normal electrochemical characterization of the samples (C/5) in standard Swagelok cells. However, the shapes of the electrochemical curves obtained at the two speeds are virtually identical, showing the same electrochemical plateaus at very similar values of electrochemical potentials. The evolution of the ^{119}Sn Mössbauer

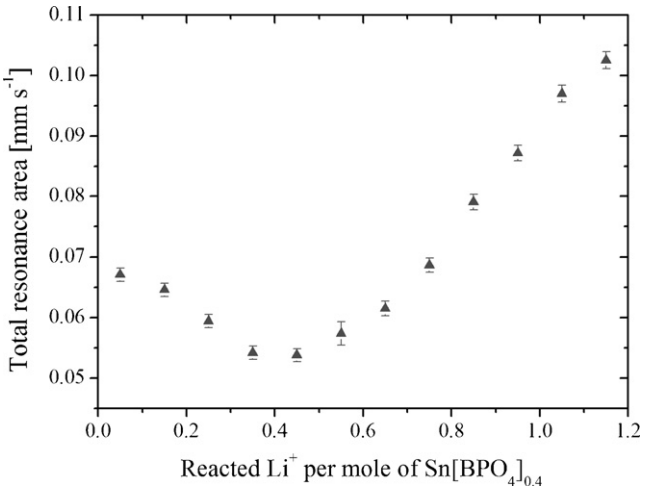

Fig. 8. Total resonance areas of the Mössbauer spectra in the region 0 → 1.2 reacted Li^+ during the first galvanostatic discharge of $Sn[BPO_4]_{0.4}$ composite.

spectra during this first part of the discharge are shown in Fig. 6. The two main effects observed in this series of spectra is the rapid fading of the peak centered at about 4 mm s^{-1}, belonging to the doublet representing divalent tin, which is completely suppressed after the reaction of 0.6 mol of Li^+ per mole of electrode material and the subsequent increase of the total resonance area of the Mössbauer spectra with the amount of reacted Li^+.

Besides, also the electrochemical curve of the 0 → 1.2 reacted Li region for the $Sn[BPO_4]_{0.4}$ composite prepared with a reaction time of 7 h can be divided in two parts: the first one, going from 0 to 0.6 mol of reacted Li^+ per mole of electrode material, is shown in Fig. 7 together with the relative amounts of divalent and metallic tin. The latter were calculated from the relative resonance areas of the respective Mössbauer spectral components and taking into account the appropriate Lamb–Mössbauer factors [7,23].

An almost linear decrease of the relative amount of Sn^{II} is observed, starting from the very beginning of the discharge. The Sn^{II} disappears completely between 0.5 and 0.6 mol of Li^+ per mole of electrode material at about 0.8 V against Li^+/Li^0. It is interesting to notice that, starting for a relative amount of 37% of Sn^{II} in the sample, 0.55 Li are necessary to completely reduce it into metallic tin. Since the divalent tin is, experimentally, completely reduced after the reaction of 0.6 mol of Li^+ per mole of electrode material, the reaction of Li with divalent tin is by far the dominant reaction during this part of the discharge, consuming most of the reacted Li.

The existence of two small plateaus (1.5 and 1.0 V vs. Li^+/Li^0, respectively), agrees well with previous results on amorphous tin composite oxides [16,26]. Essentially, Robert et al. [16], on the basis of an extensive Mössbauer study of an ATCO-type material, suggest that in this part of the discharge Li reduces the divalent tin, which is thus extruded from the amorphous interface as tin metal. The Li^+ cations formed during the reduction, known to be good glass network modifiers [27], substitute the divalent tin in the amorphous glass matrix, coordinating to oxide anions of the modified B–O–P network. The process continues down to about 0.8 V, where the lithium also reacts with the electrolyte, contributing to the formation of the solid electrolyte interface at the composite electrode.

After the reaction of 0.6 mol of Li^+ per mole of electrode material, a plateau appears at about 0.5 V vs. Li^+/Li^0, corresponding to the beginning of the transformation of metallic tin into Li_2Sn_5 and LiSn [25]. This transformation can be followed by Mössbauer spectroscopy starting from 0.6 reacted mole of Li^+ per mole of electrode material (Fig. 6), allowing one to follow the gradual vanishing of the narrow unresolved doublet centered at 2.56 mm s^{-1} of tin metal, and the simultaneous appearance of the components of the Li–Sn compositions. This phenomenon continues after 1.2 reacted Li, with the formation of a mixture of Li-rich phases (not shown).

The whole transformation of the tin species into Li–Sn compositions can be easily visualized by the evolution of the total resonance area of the Mössbauer spectra as a function of the reacted lithium amount, which is shown in Fig. 8.

In fact, the total resonance area of a given species depends on both its concentration and its relative Lamb–Mössbauer factor; therefore, a reduction of the resonance area of a sample with constant tin concentration (as is the case here) reflects the transformation of a species characterized by a high Lamb–Mössbauer factor into a new species with a relatively lower one, and vice versa.

In the first part of the reaction, a gradual attenuation of the total resonance area is observed, in agreement with the reduction of divalent tin into tin metal: in fact, divalent tin has a Lamb–Mössbauer factor about 1.8 times higher than that of metallic tin [7,23]. Considering that also the different tin alloys have increasing Lamb–Mössbauer factors with the Li content, the minimum of the total resonance area, measured at about 0.5 reacted Li, corresponds well to the presence of almost only metallic tin. This result is in good agreement with the previously described mechanism, indicating that the formation of different tin compositions starts immediately after the complete reduction of Sn^{II}.

4. Conclusions

The structure and the electrochemical mechanisms occurring at the interface phase existing between tin metal particle and borophosphate matrix in Sn–BPO_4 composite materials have been studied by *operando* Mössbauer spectroscopy. The results of this study show that the amount of interface, as well as its influence on its electrochemical behavior of the whole composite against Li metal, depends upon the reaction time between the matrix and the metal precursors, substantiating the previously proposed model [5].

Even though all composites obtained between 1 and 28 h of reaction show electrochemical activity, the best electrochemical results are obtained for the $Sn[BPO_4]_{0.4}$ composite prepared with a reaction time of 7 h sample, which shows interesting characteristics for the use as a negative electrode in future Li-ion cells.

Acknowledgments

The financial support of the agreement CNES-Région Languedoc Roussillon N 07-011380 as well as the contract ANECDOTE ANR-07-Stock-E-03-02 are largely appreciated. The authors thank Dr. P.-E. Lippens for the interesting scientific discussions.

References

[1] Y. Idota, T. Kubota, A. Matsufuji, Y. Maekawa, T. Miyasaka, Science 276 (1997) 1395–1398.
[2] S. Machill, T. Shodai, Y. Sakurai, J.-i. Yamaki, J. Power Sources 73 (1998) 216–223.
[3] D. Deng, M.G. Kim, J.Y. Lee, J. Cho, Energy Env. Sci. 2 (2009) 818–837.
[4] A. Aboulaich, M. Mouyane, F. Robert, P.-E. Lippens, J. Olivier-Fourcade, P. Willmann, J.-C. Jumas, J. Power Sources 174 (2007) 1224–1228.
[5] A. Aboulaich, M. Womes, J. Olivier-Fourcade, P. Willmann, J.-C. Jumas, Solid State Sci. 12 (2010) 65–72.
[6] A. Aboulaich, D.E. Conte, J. Olivier-Fourcade, C. Jordy, P. Willmann, J.-C. Jumas, J. Power Sources 195 (2010) 3316–3322.
[7] D.E. Conte, A. Aboulaich, F. Robert, J. Olivier-Fourcade, J.-C. Jumas, C. Jordy, P. Willmann, J. Solid State Chem. 183 (2010) 65–75.
[8] M. Mouyane, L. Aldon, M. Womes, B. Ducourant, J.-C. Jumas, J. Olivier-Fourcade, J. Power Sources 189 (2009) 818–822.
[9] W. Kündig, Nucl. Instrum. Methods 75 (1969) 336–340.
[10] J.B. Leriche, S. Hamelet, J. Shu, M. Morcrette, C. Masquelier, G. Ouvrard, M. Zerrouki, P. Soudan, S. Belin, E. Elkaïm, F. Baudelet, J. Electrochem. Soc. 157 (2010) A606–A610.
[11] V.I. Goldanskii, R.H. Herber, Chemical Applications of Mössbauer Spectroscopy, Academic Press, New York, 1968, p. 701.

[12] N.N. Greenwood, T.C. Gibb, Mössbauer Spectroscopy, Chapman and Hall Ltd., London, UK, 1971.
[13] U. Gonser, in: H.K.V. Lotsch (Ed.), Topics in Applied Physics, Springer-Verlag, Berlin, 1975, p. 240.
[14] G.K. Shenoy, F.E. Wagner, Mössbauer Isomer Shifts, Nort-Holland, Amsterdam, 1978, p. 956.
[15] G.J. Long, in: J.P.J. Fackler (Ed.), Modern Inorganic Chemistry, Plenum Press, New York, 1984, p. 688.
[16] F. Robert, F. Morato, J. Chouvin, L. Aldon, P.-E. Lippens, J. Olivier-Fourcade, J.-C. Jumas, B. Simon, P. Biensan, J. Power Sources 119–121 (2003) 581–584.
[17] Z. Edfouf, M.J. Aragon, B. Leon, C.P. Vicente, J.L. Tirado, J. Phys. Chem. C 113 (2009) 5316–5323.
[18] A.B. Atkarskaya, V.I. Kiyan, Glass Ceram. 59 (2002) 119–122.
[19] J.L.C. Rowsell, J. Gaubicher, L.F. Nazar, J. Power Sources 97–98 (2001) 254–257.
[20] M. Gunaltun, J.J. Rameau, Electrochim. Acta 29 (1984) 737–744.
[21] S. Elbers, W. Strojek, L. Koudelka, H. Eckert, Solid State Nucl. Magn. Reson. 27 (2005) 65–76.
[22] D. Raskar, M.T. Rinke, H. Eckert, J. Phys. Chem. C 112 (2008) 12530–12539.
[23] M.T. Sougrati, S. Jouen, B. Hannoyer, Hyperfine Interact. 167 (2006) 815–818.
[24] I.A. Courtney, J.S. Tse, O. Mao, J. Hafner, J.R. Dahn, Phys. Rev. B 58 (1998) 15583–15588.
[25] P.-E. Lippens, L. Aldon, C.-M. Ionica-Bousquet, F. Robert, J. Olivier-Fourcade, J.-C. Jumas, Mater. Res. Soc. Symp. Proc. 835 (2004) K10–11.
[26] M. Behm, J.T.S. Irvine, Electrochim. Acta 47 (2002) 1727.
[27] N.K. Karan, B. Natesan, R.S. Katiyar, Solid State Ionics 177 (2006) 1429–1436.